



Article

Effects of Fly Ash Dosage on Shrinkage, Crack Resistance and Fractal Characteristics of Face Slab Concrete

Lei Wang^{1,2,*} , Zhiqiang Yu³, Bo Liu¹, Feng Zhao¹, Shengwen Tang⁴ and Minmin Jin²

¹ School of Intelligent Construction, Wuchang University of Technology, Wuhan 430002, China; 120100519@wut.edu.cn (B.L.); 120100520@wut.edu.cn (F.Z.)

² College of Materials Science and Engineering, Xi'an University of Architecture and Technology, Xi'an 710055, China; jmm@xauat.edu.cn

³ Yangtze River Scientific Research Institute, Wuhan 430010, China; yuzq@mail.crsri.cn

⁴ State Key Laboratory of Water Resources and Hydropower Engineering Science, Wuhan University, Wuhan 430072, China; tangsw@whu.edu.cn

* Correspondence: wanglei535250684@xauat.edu.cn

Abstract: The crack resistance of face slab concretes to various shrinkages is crucial for the structural integrity and the normal operation of concrete-faced rockfill dams (CFRDs). In this work, the effects of fly ash with four dosages (i.e., 10%, 20%, 30% and 40%) on the drying shrinkage, autogenous shrinkage and the cracking resistance of face slab concrete were studied. Besides, the difference in shrinkage behavior due to fly ash addition was revealed from the viewpoint of the pore structure and fractal dimension of the pore surface (D_s). The findings demonstrate that (1) the incorporation of 10–40% fly ash could slightly reduce the drying shrinkage by about 2.2–13.5% before 14 days of hydration, and it could reduce the drying shrinkage at 180 days by about 5.1–23.2%. By contrast, the fly ash addition could markedly reduce the autogenous shrinkage at early, middle and long-term ages. (2) Increasing fly ash dosage from 0 to 40% considerably improves the crack resistance of concrete to plastic shrinkage. Nevertheless, the increase in fly ash dosage increases the drying-induced cracking risk under restrained conditions. (3) The pore structures of face slab concrete at 3 and 28 days become coarser with the increase in fly ash dosage up to 40%. At 180 days, the pore structures become more refined as the fly ash dosage increases to 30%; however, this refinement effect is not as appreciable as the fly ash dosage increases from 30% to 40%. (4) The D_s of face slab concrete is closely related with the concrete pore structures. The D_s of face slab concrete at a late age increases from 2.902 to 2.946 with increasing of the fly ash dosage. The pore structure and D_s are closely correlated with the shrinkage of face slab concrete. (5) The fly ash dosage around 30% is optimal for face slab concretes in terms of lowering shrinkage and refining the pore structures, without compromising much mechanical property. However, the face slab concretes with a large fly ash dosage should be well cured under restrained and evaporation conditions at an initial hydration age.

Keywords: concrete face slab; shrinkage; crack resistance; pore; fractals



Citation: Wang, L.; Yu, Z.; Liu, B.; Zhao, F.; Tang, S.; Jin, M. Effects of Fly Ash Dosage on Shrinkage, Crack Resistance and Fractal Characteristics of Face Slab Concrete. *Fractal Fract.* **2022**, *6*, 335. <https://doi.org/10.3390/fractalfract6060335>

Academic Editor: Wojciech Sumelka

Received: 30 May 2022

Accepted: 15 June 2022

Published: 16 June 2022

Publisher's Note: MDPI stays neutral with regard to jurisdictional claims in published maps and institutional affiliations.



Copyright: © 2022 by the authors. Licensee MDPI, Basel, Switzerland. This article is an open access article distributed under the terms and conditions of the Creative Commons Attribution (CC BY) license (<https://creativecommons.org/licenses/by/4.0/>).

1. Introduction

The concrete faced rockfill dam (CFRD) is one kind of rockfill dam, consisting of a rockfill body as a supporting body and the concrete face slabs as the anti-leakage structures. CFRD is considered to be a safe, low cost and reliable dam type [1–6]. According to the statistical data in the existing literature [3,4,7], there are more than 600 CFRDs around the world nowadays, and more than 50% of them are in China. Currently, motivated by the Chinese policies, lots of pumped storage power stations with the CFRD-dam-type will be constructed in China in the next few years [7,8]. The concrete face slabs, which are typical thin (commonly within 0.4–1.0 m in thickness) and large concrete members with an extremely high surface to volume ratio, are susceptible to cracking due to the drying and thermal stresses [5,9], as well as the constraint of the dam foundation, etc. [1,5,10]. The weak

early tensile strength of concrete may further increase the crack risk of the concrete face slabs. Taking into account that the face slab concrete is the dominate anti-leakage structure of CFRDs, the cracks in concrete face slabs would inevitably cause leakage and weaken the structural integrity and the normal operation of CFRDs [11]. Moreover, the cracks in concrete favor the ingress of deleterious ions, which could cause durability problems. Therefore, reducing the shrinkage and enhancing the crack resistance of face slab concrete are crucial concerns in designing and building constructing CFRDs in practice [1,5,6,10].

It is widely reported that fly ash could reduce the shrinkage as well as the potential crack risk of concrete [12–16]. Fly ash is a by-product of the thermal power plant, the main constituents of which are silicate glassy phases, crystalline phases and some impurities [17–20]. Fly ash could densify the cementitious matrix and refine the microstructure because of its filler effect and pozzolanic effect, which could, in turn, improve the resistance of concrete to various shrinkages [15,21,22]. Currently, fly ash is widely used in hydraulic mass concrete structures to reduce the temperature rise and the resulting thermal shrinkage [23–25]. Moreover, fly ash is also suggested to be utilized in concrete-resulting face slabs, as specified in DL/T 5016 (Chinese standard for designing concrete-faced rockfill dams) [26]. For instance, fly ash with a dosage of around 30%, by weight of binder, has been used in concrete face slabs in Fengning CFRD, the largest pumped storage power station in the world, to reduce the shrinkage and to enhance the crack resistance of face slab concretes [27]. In addition, the effects of fly ash dosage on durability (i.e., permeability and frost resistance) of face slab concretes were systematically studied by Woo, S.K. et al. [9,28], who found that a 15% fly ash dosage yields the most effective durability level for face slab concrete. However, there are no systematical studies so far regarding the effects of fly ash dosage on shrinkage behavior and crack resistance of face slab concretes.

Fractal geometry provides an effective means to study the performance of concrete. Fractal geometry links the performance of concretes with their microstructures [29]. The microstructures of cement composites, including the pore structures and meso-structures, such as the air voids, as well as the morphological features of powders and the fracture surfaces, commonly present extremely complex and irregular features, which are difficult to describe in terms of geometry but can be investigated by fractal geometry [30–32]. Several fractal dimensions, including the fractal dimensions of the pore surface, pore volume, tortuosity, air void, fracture surface and cracks, as well as the particle size distribution, etc., have been developed and applied to study the different properties of cement composites [31,33,34]. These fractal dimensions have quite different physical meanings. The fractal dimension of the pore surface is one key parameter of fractal geometry, which could characterize the complexity and heterogeneity of the pore structures of concrete. It is well-known that the pore structure strongly affects the mechanical properties, shrinkage behavior and durability of concrete [35,36]. The fractal dimension of the pore surface of concrete has been proven to be closely associated with the strength, permeability and frost resistance of concrete, etc. [32,37]. For example, it was reported that the enhancement of concrete frost resistance is accompanied by the increase in the pore surface fractal dimension (D_s) [37]. Jin et al. [31] revealed that the mechanical properties of cement mortars increase with the pore structure fractal dimensions. Nevertheless, to date, there have been no studies concerning the effects of fly ash dosage on the fractal features of face slab concrete.

To remedy the two inadequacies mentioned above, the influences of fly ash with four dosages, namely 10%, 20%, 30% and 40%, on the drying shrinkage, autogenous shrinkage and the crack resistance of face slab concretes were studied and compared. In addition, the difference in shrinkage behavior caused by fly ash addition was revealed from the viewpoint of pore structures and fractals. The findings presented in this paper may provide a new perspective on the effects of fly ash dosage on shrinkage properties of face slab concretes and provide a theoretical guide for the selection of proper fly ash dosage in designing face slab concretes with a desirable cracking resistance.

2. Materials and Methods

2.1. Materials

In this study, a Portland cement (CEM I 42.5, complying with the Chinese national standard GB 175) with a 28-day compressive strength of 46.5 MPa and an ASTM Type F fly ash were used. The physical characteristics of Portland cement and fly ash are exhibited in Table 1. The oxide compositions of cement and fly ash, as determined by the X-ray fluorescence (XRF) technique, are also listed in Table 1. The limestone was manufactured into coarse and fine aggregates. The specific gravity of these aggregates is 2.68. The fineness modulus of the fine aggregate is 2.71. The coarse aggregates have a particle size range of 5–40 mm.

Table 1. Physical characteristics and oxide compositions of cement and fly ash.

Oxides	Oxide Composition (wt. %)	
	CEM I PC	Fly Ash
CaO	62.72	2.94
SiO ₂	20.32	54.54
Fe ₂ O ₃	4.46	10.18
Al ₂ O ₃	4.42	24.78
MgO	3.92	2.94
SO ₃	2.37	0.37
R ₂ O *	0.41	1.04
Loss on ignition (%)	1.04	2.18
Physical Properties		
Specific gravity	3.22	2.32
Specific surface area by Blaine method (m ² /kg)	332	386
Fineness (% retain in 45 μm)	8.4	6.8
Strength activity index	-	78

* Alkali content (R₂O) = Na₂O + 0.658K₂O.

2.2. Mix Proportions of Face Slab Concrete

The concrete mixture proportions were designed conforming to DL/T 5016 (Chinese design code for concrete-faced rockfill dams) [26] and the volume method described in DL/T 5330 (Chinese code for the mix design of hydraulic concrete) [38]. The face slab concretes were designed to have a compressive strength range of 35.0–45.0 MP at 28 days, which is normally adopted in practical CFRDs engineering. For all of the concretes, the W/B, sand to aggregate ratio and the water amount were determined as 0.37, 33% and 123 kg/m³, after lots of pre-experiments. The superplasticizer with a dosage of 0.7–1.1%, by weight of binder, was added to obtain a concrete slump value between 55–65 mm. Five concretes containing fly ash with dosages of 0, 10%, 20%, 30% and 40% (by weight of cementitious materials) were prepared. It should be noted that the fly ash dosage up to 50–70% was adopted in hydraulic mass concrete, and the objective of fly ash utilization in such cases was to reduce the temperature rise and thermal crack risk of mass concrete [23,24]. Nevertheless, fly ash under the dosage of 40% was utilized in this study, since higher fly ash dosages could significantly lower the 28-day mechanical strength of face slab concrete. Besides, different from mass concrete, the aim of fly ash utilization in thin concrete face slabs is to reduce shrinkage. These mixtures were designated as C0, CF10, CF20, CF30 and CF40, respectively. The detailed mixture proportions of face slab concretes are shown in Table 2.

Table 2. Mix proportion of face slab concretes.

Designations	W/B Ratio	Fly Ash Dosage (wt.%)	Mix Proportions (kg/m ³)					Slump (mm)	
			Water	Cement	Fly Ash	Sand	Coarse Aggregate		Super Plasticizer
C0	0.4	0	122	305	0	630	1339	1.8	65
CF10	0.4	10	122	293	12	631	1340	2.4	55
CF20	0.4	20	122	281	24	631	1341	2.7	51
CF30	0.4	30	122	293	12	631	1340	2.1	62
CF40	0.4	40	122	281	24	631	1340	2.4	57

2.3. Test and Calculation Methods

2.3.1. Compressive and Splitting Tensile Strength Test of Face Slab Concretes

The compressive strength and splitting tensile strength of face slab concretes were tested at 3, 28 and 180 days, by using a 300 kN capacity testing system, conforming to DL/T 5150 (Chinese test code for hydraulic concrete) [39]. The fresh concrete was cast into cubic molds sized 150 × 150 × 150 mm and maintained under laboratory conditions. After 24 h, they were demolded and kept in a foggy room at around 20 °C and relative humidity (RH) above 95%. For the determination of each compressive strength and splitting tensile strength result, six and three specimens were tested, respectively, and the average value was reported as the final result.

2.3.2. Shrinkage Behavior Measurements

CFRDs in the north and west parts of China commonly suffer from severe drying actions. In the drying conditions, the thin concrete face slab with a large surface area and a relatively low W/B ratio is easy to shrink, exhibiting mainly drying and autogenous shrinkage. The drying shrinkage is due to the water evaporation from the connected concrete pores in the drying process, and the autogenous shrinkage is owed to the self-desiccation in concrete pores caused by cement hydration [15,22].

For the determination of drying shrinkage according to DL/T 5150 [39], three concrete prism samples with a size of 100 mm × 100 mm × 515 mm were measured, and the average value was reported for each concrete mixture. During the test, the initial length of the prism samples was recorded immediately once the specimens were demolded, by using digital gauges. The concrete prisms were subsequently stored in a drying room (about 20 °C and 50% RH). Then, the length changes of the concrete prisms were continuously measured and recorded up to 180 days. The drying shrinkage can be determined based on the length change data.

During the autogenous shrinkage test complying with DL/T 5150, three concrete samples for each proportion with a dimension of Φ 200 mm × 500 mm were measured, and the average value was reported. Before the test, the barrels made of a galvanized sheet should be prepared. After a strain meter was horizontally fixed in the center of the barrels, the fresh concrete was put in the barrels compactly. Subsequently, the barrel was soldered and sealed to avoid water loss from the concrete during the whole test process. After that, the barrels were stored in the ambient environment at about 20 °C. Once the test began, the data-acquiring system connected to the embedded strain meter through a cable could record the strain data continuously until 180 days.

2.3.3. Cracking Resistance Test of Concrete

Currently, several methods have been developed to test the crack resistance of concrete, including the concrete slab test [40] and the restrained concrete ring test, etc. [12,41].

The Concrete Slab Test

The plastic shrinkage-induced cracking is very common for concrete structures, particularly for those with large surface areas and a small thickness, i.e., concrete slab, thin surface repair and tunnel lining, etc. [40,42]. The plastic shrinkage mainly occurs during

the first several hours after concrete casting, which results from the evaporation of mix water. If concrete is restrained, the rapidly-developed plastic shrinkage would produce great tensile stresses and even severe cracking in young concrete, which is still in the plastic stage [42,43].

To probe the crack risk of face slab concrete induced by the plastic shrinkage, the slab test was performed, conforming to CCES 01-2004 (Chinese design and construction guide for the durability of concrete structures) [44]. At the beginning of the test, the coarse aggregate with a size larger than 20 was sieved from the fresh concrete. Thereafter, the sieved concrete was cast into the mold with a size of 60 cm × 60 cm × 6 cm (as shown in Figure 1a), consolidated and finished. After that, the specimens stored in a drying room at about 20 °C and 50% RH were exposed to a strong wind, in order to accelerate the evaporation process. The concrete slabs were continuously monitored up to 24 h. After 24 h of wind blowing, the initial cracking time, the width and length of each crack and the total number of cracks that appeared in each concrete slab were recorded. An example of cracking in this test is given in Figure 1b, in which the enlarged image of a crack is shown in Figure 1c. Then, the key parameters of cracks can be obtained according to Equations (1)–(3).

$$\alpha_c = 1/(2N) \sum_i^N W_i L_i \quad (1)$$

$$N_{unit} = N/A \quad (2)$$

$$A_c = \alpha_c N_{unit} \quad (3)$$

where α_c refers to the mean area of the cracks, mm²; N_{unit} denotes the number of cracks per unit area, /m²; A_c represents the total area of cracks per unit area, mm²/m²; N refers to the total number of cracks; L_i and W_i represent the length and width of i th crack, respectively, mm; A is the slab area, which equals 0.36 m².

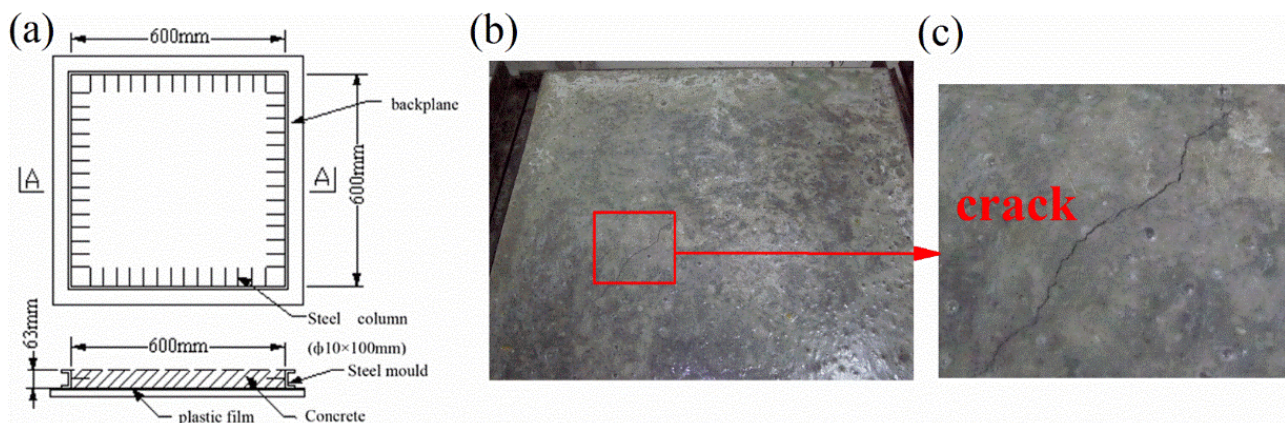


Figure 1. The illustration of the slab test: (a) the steel mold, (b) specimen and (c) crack.

The crack resistance of concrete to plastic shrinkage can be divided into five levels, namely Level I to Level V, based on whether the four criteria can be satisfied, as follows: (1) only has very tiny cracks, (2) $\alpha_c < 10$ mm², (3) $N_{unit} < 10$ /m² and (4) $A_c < 100$ mm²/m². Level I denotes the best crack resistance, which means the concrete satisfies all the four criteria above. The crack resistance of levels II, III, IV and V refer to the concrete that satisfies three, two, one and none of the criteria, respectively.

The Restrained Concrete Ring Test

The shrinkage of face slab concretes is commonly restrained by foundations, which may lead to the generation of tensile stresses. The face slab concretes under strong constraints would crack once the tensile stresses are larger than the tensile strengths of concrete [12,45]. The restrained concrete ring test, according to ASTM C 1581 [46], is a widely

accepted technique to test the cracking resistance of concrete to restrained shrinkage at an early age [12,41,47].

According to ASTM C 1581, the outer size, inner size and thickness of the concrete ring specimens are 406 mm, 330 mm and 152 mm, respectively, as shown in Figure 2. Before casting the specimens, the coarse aggregate sized larger than 20 mm should be removed from the fresh concrete. The outer steel ring should be demolded after the specimens are cured for 24 h. Then, the top surface and the bottom surfaces of the specimens were painted and covered with a layer of sealant in order to guarantee that the drying could only act on the outer circumferential surface. After that, the ring specimens were stored under a drying condition at about 20 °C and 50% RH, thereafter the initial cracking time of the specimens was monitored and recorded. Three ring specimens were tested for each concrete proportion, and the mean value was used as the final result. More detailed testing procedures were exhibited in the study [24].



Figure 2. The picture of the restrained concrete ring test.

2.3.4. Pore Structure Parameters by Mercury Intrusion Porosimeter (MIP)

The MIP porosimeter (AutoPore IV 9500 type, manufactured by Micromeritics Instruments Corporation, Norcross, GA, USA) was used to probe the pore structures of concrete. This porosimeter has a mercury intrusion pressure from 0 to 414 MPa. The pore size ranging from ~2 nm to 10 μm can be tested by this porosimeter. The concrete pieces used for MIP tests were obtained by cutting the internal part of concrete into small pieces with a size about 5–8 mm. Before the MIP tests, the coarse aggregates were removed from the small pieces. Three cubic pieces were used for an MIP test, in order to prevent the experimental error caused by sample size or sample quality variations.

2.3.5. Fractal Method

It is widely reported that the shrinkage behavior of concrete is dominated by the pore structure [48,49]. The pores in concretes are extremely complex and heterogenous. It is generally agreed that the complexity and heterogeneity of the pores in concrete can be studied in terms of the fractal dimension. In order to better understand the effects of fly ash on pore structures and shrinkage of concrete, the fractal characteristics of face slab concrete were studied.

In this work, the fractal dimension of pore surface (D_s) was used to characterize the pore structures. D_s can be calculated using a thermodynamic fractal model [50,51] and MIP results.

The fundamental of this thermodynamic model [50,51] is that during the MIP test, the accumulated injection work on mercury (W_n) is logarithmically related with the total injected mercury volume (V_n), as indicated by Equation (4):

$$\ln \frac{W_n}{r_n^2} = D_s \ln \frac{V_n^{1/3}}{r_n} + C \quad (4)$$

where r_n is the pore radius, m; n represents the n -th mercury injection; C is a regression constant. W_n can be determined by Equation (5):

$$W_n = \sum_i^n p_i \Delta V_i \quad (5)$$

where the index i is the i -th mercury injection, which ranges between 1 and n ; p_i represents the mercury pressure, Pa; V_i denotes the volume of mercury injected at the i -th injection, m^3 .

The values of W_n , V_n , $\ln \frac{W_n}{r_n^2}$ and $\ln \frac{V_n^{1/3}}{r_n}$ can be calculated directly from the MIP results and Equation (5). After that, D_s can be easily determined, which is the slope of the straight line in Equation (4). The correlation coefficient (R^2) of the fitted line can be also obtained.

3. Results and Discussion

3.1. Compressive and Splitting Tensile Strength

The compressive strength and splitting tensile strength of face slab concretes were tested at 3, 28 and 180 days, and the results are illustrated in Figure 3. The error bars of the strength results are also shown in Figure 3.

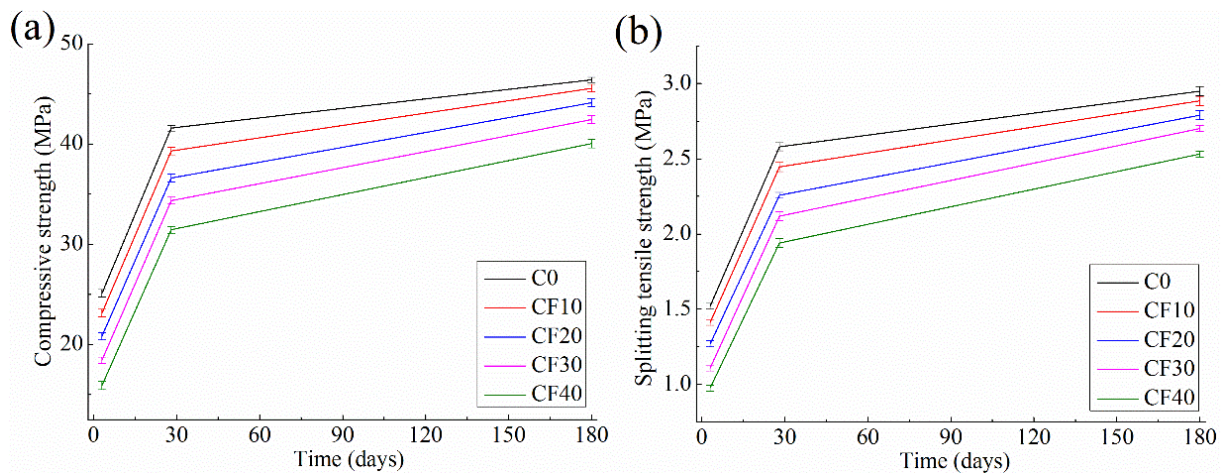


Figure 3. Strengths of face slab concretes at 3, 28 and 180 days: (a) compressive strength and (b) splitting tensile strength.

Figure 3 shows that both the compressive strength and splitting tensile strength of face slab concretes increased as the hydration time increased. Furthermore, Figure 3 exhibits that the fly ash dosage significantly affected the mechanical property of face slab concretes at an early age. Specifically, the three-day compressive strength of face slab concrete was reduced by 7.8%, 17.0%, 26.5% and 36.6% after the addition of 10%, 20%, 30% and 40% dosage of fly ash, respectively. Similar reductions, which were 7.1%, 16.5%, 27.1% and 35.8%, were also found for the three-day splitting tensile strength after the addition of 10%, 20%, 30% and 40% fly ash, respectively. These reductions can be explained by the weak reactivity of fly ash at an early age and the dilution effect of fly ash [23–25].

Nevertheless, as shown in Figure 3, with the progress of hydration, the difference in mechanical property among all the concretes added with fly ash became smaller and smaller. For instance, the 28-day compressive strengths of face slab concretes added with 10–40% fly ash were about 5.5–22.4% smaller than that of C0 concrete. Besides, the CF10 and CF20

concretes have similar 180-day strengths with C0 concrete, while the CF30 and CF40 concretes have about 8.5% and 13.7% smaller 180-day compressive strengths compared with the C0 one, respectively. Similar trend could be found for the splitting tensile strength, demonstrating that the pozzolanic reaction of fly ash at the long-term hydration age is beneficial for the strength improvement of concrete. These results are in good agreement with the findings reported by Hu et al. [22] and Malhotra et al. [52], Yoon et al. [28] and Matos et al. [53], which revealed obvious improvements in long-term mechanical properties of fly ash concrete. From a detailed review of the current literature, it can be summarized that the reaction degree of fly ash was less than 4% at 3 days [54], 9–23% at 28 days [14,54–57] and 26–33% at 180 days [14,54], depending on the glassy content, chemical composition and fineness of fly ash. Overall, the improvement in the mechanical property is owed to the pozzolanic reaction between fly ash and $\text{Ca}(\text{OH})_2$, which could produce lots of secondary C-S-H, resulting in refined pore structures and enhanced late-age strength [24,56,58].

3.2. Volume Deformation

3.2.1. Drying Shrinkage

Figure 4 presents the drying shrinkage values of face slab concrete added with a 0–40% dosage of fly ash up to 180 days. From Figure 4, within the first two weeks, the drying shrinkage increased quickly, and after that, it developed relatively slowly until 180 days. As concluded by Hu et al. [22] and Yang et al. [59], the water loss from concrete pores during the evaporation process at an early age may lead to the generation of capillary stresses, which is the main reason for the rapid increase in drying shrinkage at the early hydration age.

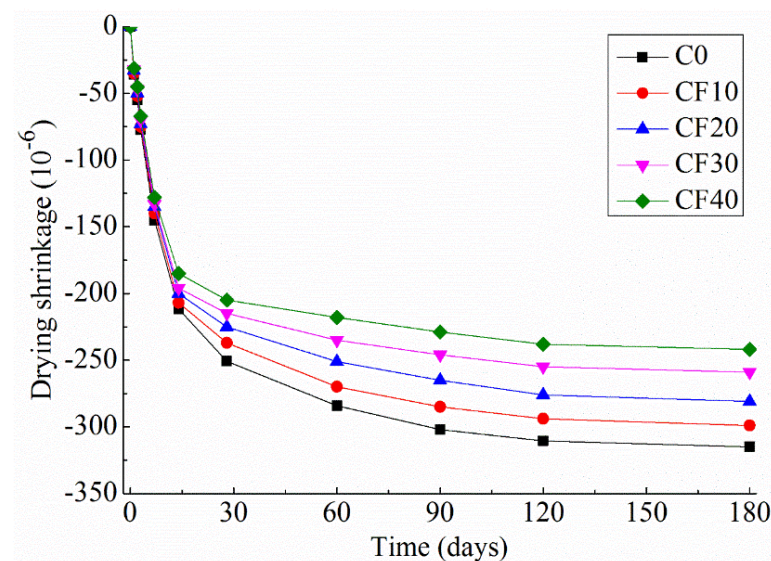


Figure 4. Drying shrinkage of face slab concretes with various fly ash dosages.

In addition, Figure 4 displays that the fly ash dosage has a more notable influence on the long-term drying shrinkage than on the early age one. In Figure 4, the drying shrinkage curves seemed to be overlapped before 14 days. The comparison of the data in Figure 4 shows that the fly ash addition could somewhat slow down the early shrinkage development, but the difference in drying shrinkage values among all the concretes added with 0–40% dosages of fly ash was not so significant. Specifically, the additions of 10%, 20%, 30% and 40% fly ash reduced the drying shrinkage between 3 and 14 days by about 2.2–3.1%, 5.5–5.7%, 7.4–9.6% and 12.6–13.5%, respectively. This slight reduction in early drying shrinkage was probably because the addition of fly ash lowers the cement content and slows down the increment of shrinkage [12,15].

Besides, there is another important mechanism responsible for the slight reduction in early drying shrinkage. It is worthy to note that drying shrinkage of concrete is governed by the water loss from concrete pores during the evaporation process [13,60]. At an early

hydration time, fly ash hardly takes part in the pozzolanic reaction, and the early pore structure of concrete is dominated by the water amount in the concrete proportion [15]. Note that the water amount in all of the face slab concrete proportions was the same, i.e., 122 kg/m^3 , so it is not surprising that the evaporation effects on the concretes added with 0–40% fly ash were almost the same under the same drying conditions during the initial drying period. Therefore, the reduction in early drying shrinkage due to fly ash addition was slight, and all of the face slab concretes exhibited similar drying shrinkage values at an early age.

Moreover, Figure 4 indicates that the fly ash addition reduced the drying shrinkage of face slab concrete hydrated between 28 days and 180 days obviously, and the drying shrinkage declined obviously with the increase in the fly ash dosage. Specifically, the incorporations of 10%, 20%, 30% and 40% fly ash reduced the drying shrinkage at 28 days by about 5.5%, 10.3%, 14.6% and 18.4%, respectively. Similarly, it reduced the 180-day drying shrinkage by about 5.1%, 10.8%, 17.8% and 23.2%, respectively, compared with the C0 concrete. The results are in agreement with other researchers [15,21,22], who reported that the drying shrinkage can be effectively lowered in the presence of fly ash and that this effect would be enhanced as the fly ash dosage increases. These reductions in drying shrinkage can be explained as follows. The decrease in cement content due to fly ash addition is the first reason. It is widely accepted that the cement pastes are the source of concrete shrinkage [15]. The fly ash addition reduces the cement content in the mixture and consequently slows down the development of shrinkage [12,15]. Consequently, the face slab concretes with a higher fly ash dosage will generate a lower shrinkage. Secondly, as hydration proceeds, the pore structure of concrete could be optimized due to the pozzolanic reaction of fly ash at a middle and late age. The improved pore structure contributes to the enhancement of resistance to shrinkage to some degrees [61,62].

3.2.2. Autogenous Shrinkage

Figure 5 depicts the autogenous shrinkage development of face slab concrete added with 0–40% dosage of fly ash up to 180 days. The autogenous shrinkage of concrete is owed to the self-desiccation caused by the water consumption during the cement hydration under sealed conditions, without any moisture exchange [13,59,60]. It can be observed from Figure 5 that there is a rapid increase in autogenous shrinkage during the first 28 days of hydration. This is a widely reported experimental phenomenon, since cement hydrates with water quickly during the first 28 days, which could produce a rapid development of autogenous shrinkage.

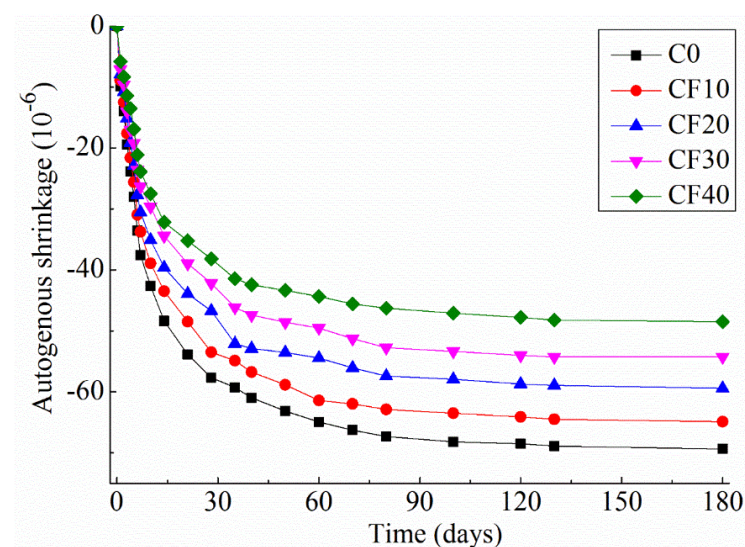


Figure 5. Autogenous shrinkage of face slab concretes with various fly ash dosages.

Figure 5 also indicates the fly ash dosage significantly affects the autogenous shrinkage development. Different from the effects on drying shrinkage, fly ash could not only reduce the long-term autogenous shrinkage, but also effectively reduce the early age autogenous shrinkage. For instance, nearly 9.4%, 22.2%, 27.9% and 41.3% of three-day autogenous shrinkage is lowered due to the addition of 10%, 20%, 30% and 40% fly ash, respectively. Similarly, the 180-day autogenous shrinkage is reduced by about 6.5%, 14.4%, 21.8% and 30.1% due to the incorporation of 10%, 20%, 30% and 40% fly ash, respectively. Some other studies [15,16] also proved that the autogenous shrinkage of concrete would be gradually lowered with increasing the fly ash dosage.

The reduction effect on autogenous shrinkage due to fly ash addition may be explained by the following two reasons. One is the dilution effect of fly ash. Considering the inert nature of fly ash at an early age, as well as there being no water loss during the autogenous shrinkage test, cement content in concrete plays a predominant role in determining the autogenous shrinkage [14,15]. The addition of fly ash reduces the cement content proportionally, as shown in Table 2, which leads to less water consumption during the hydration process. As a consequence, the capillary pressure and self-desiccation of concrete can be eased effectively after the fly ash addition, reducing the autogenous shrinkage [16,63,64]. The other reason is the pozzolanic reaction of fly ash, which could refine the pore structure of concrete, especially at a long-term age [61,62]. The same reduction in long-term autogenous shrinkage was observed for self-compacting concrete added with 35–65% fly ash, conducted by Stefanus and Aditya [15]. They noted that the pozzolanic reaction of fly ash would refine the pore structures and reduce the pores size of concrete and therefore reduce the concrete autogenous shrinkage. Based on the aforementioned reasons, the face slab concrete with a higher fly ash dosage exhibits a larger reduction in autogenous shrinkage.

Taking into account that the drying and autogenous shrinkage of face slab concretes considerably takes place at an early hydration time, the relatively high fly ash dosage of 30–40% is optimal for face slab concretes in terms of lowering shrinkage.

3.3. Cracking Resistance

3.3.1. The Concrete Slab Test Result

The initial cracking time, average area of cracks (α_c), number of cracks per unit area (N_{unit}), the total area of cracks per unit area (A_c), and the crack resistance of face slab concrete obtained from the slab test are listed in Table 3. Table 3 indicates that the initial cracking time of all the specimens was within the initial 5–9 h after concrete mixing. It can be noted that the concrete specimens were in the plastic stage when the cracking occurred. As stated by Rao [43], the evaporation of mix water during the plastic stage may produce the plastic shrinkage. Under the restrained conditions, the plastic shrinkage could result in the rapidly-developed tensile stresses and even severe cracking.

Table 3. The slab test results of face slab concrete with different fly ash dosages.

Notation	Cracking Time (min)	α_c (mm ²)	N_{unit} (/m ²)	A_c (mm ² /m ²)	Crack Resistance Level
C0	330	43.6	12	523.2	V
CF10	410	31.6	7	221.2	IV
CF20	480	15.6	6	93.6	III
CF30	505	8.6	2	17.2	I
CF40	540	8.4	3	25.2	I

Table 3 indicates that the incorporation of fly ash declines the initial cracking time and lowers the values of α_c , N_{unit} and A_c , implying that the crack resistance of face slab concretes to plastic shrinkage is largely enhanced. In addition, Table 3 exhibits that the increase in fly ash dosage obviously enhances the crack resistance of face slab concretes to plastic shrinkage, and the addition of 40% fly ash exhibits the best performance in this regard. For instance, CF10 concrete presents an initial cracking time of 410 min and a

level “IV” crack resistance, while the initial cracking time of CF40 concrete is prolonged to 540 min, and its crack resistance level is improved to “level I”.

The improvement in crack resistance to plastic shrinkage can be attributed to the extra free water when the fly ash is used or when the fly ash dosage is increased. Since the fly ash particles are spherical and have a smooth surface texture, their water absorption capacity of fly ash particles is obviously weaker than the cement particles, which have irregular shapes and rough textures [65]. In addition, the addition of fly ash produces a larger effective W/B in the concrete mixtures due to its inert nature at an early age and dilution effect. The synergy effect of the weak water absorption capacity of fly ash and a larger effective W/B will produce more bleeding water in the concrete mixture compared with the control concrete. As stated by Banthia and Gupta [40] and Amoudi et al. [42], under the evaporation conditions, the mix water in fresh concretes would be lost first, and then the pore water would start to be lost. Thus, the evaporation of some mix water could moderate the capillary pressure development and mitigate the plastic shrinkage under the severe evaporation action. Due to the proper “protection” of extra mix water, the strong evaporation action would reduce the crack risk and produce a longer cracking time of face slab concrete added with a higher fly ash dosage.

3.3.2. Restrained Concrete Ring Test Result

During the restrained concrete ring test, the drying-induced shrinkage of face slab concretes is restrained by the steel ring, leading to the development of tensile stresses. The cracks in the concrete slabs would appear when the tensile stresses are larger than the tensile strengths of concrete. The restrained ring test results of concrete rings added with 0–40% fly ash are shown in Figure 6.

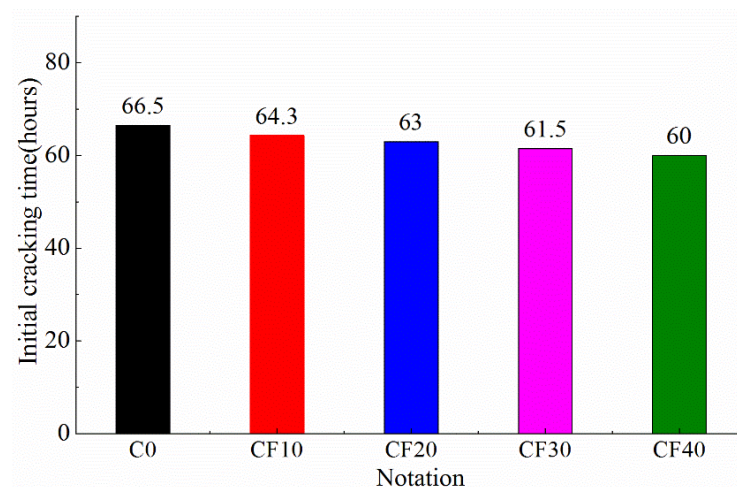


Figure 6. The restrained ring test results of face slab concretes with various fly ash dosages.

From Figure 6, the average initial cracking time of face slab concretes with various fly ash dosages was exhibited in the following sequence: 66.5 h (C0) > 64.3 h (CF10) > 63.0 h (CF20) > 61.5 h (CF30) > 60 h (CF40), indicating that the increase in fly ash dosage gradually shortened the initial cracking time and weakened the crack resistance to drying shrinkage. These results appear to be in contradiction with the drying shrinkage results above, which indicate that fly ash addition could slightly reduce the drying shrinkage value, or with the previous ring test results reported by Pipat et al. [12], who reported that the increase in fly ash content until 50% effectively delayed the initial crack time of the restrained concrete rings.

These seemingly conflicting results may be understood from two aspects: (1) as revealed in Section 3.2.1, although the reduced amount of cement by fly ash incorporation slightly reduces the drying shrinkage of concrete at an early age, due to the dominate evaporation mechanism, the shrinkage of concrete caused by drying is much larger than the shrinkage caused by cement hydration. As a result, the drying shrinkage curves

are somewhat overlapped before 14 days. Therefore, it is reasonable to assume that the constraints acted by the steel rings are almost the same, producing similar stress development in the concrete rings. Considering the decrease in the early tensile strength of concrete as fly ash dosage increased, under the same evaporation action and constraint conditions, the CF40 concrete with the weakest tensile strength exhibited the weakest early cracking resistance to drying shrinkage, while the C0 concrete with the largest tensile strength displayed the best crack resistance to drying shrinkage. (2) The major difference in the ring tests between Pipat et al. [12]'s work and the current work is the experimental conditions. In Pipat et al. [12]'s work, after the specimens being demolded, the concrete rings were wetly cured for 3–7 days. Then, the rings were directly exposed to the air in the laboratory, rather than in the drying room, which was adopted in this work. As a consequence, the shrinkage of the rings in their work was mainly owing to the cement hydration, rather than the evaporation mechanism. Due to different shrinkage mechanisms, a weaker early cracking resistance was observed for concrete with a higher fly ash dosage in this study.

To sum up, under restrained conditions, the drying-induced crack risk of face slab concrete increased with increasing the fly ash dosage. Hence, the concrete face slabs containing a large dosage of fly ash should be well cured at an early age if they are restrained and exposed to severe evaporation conditions.

3.4. MIP Result

Table 4 exhibits the most probable pore size, porosity and the pore size distribution of face slab concretes containing various fly ash dosages hydrated at 3, 28 and 180 days. The classification proposed by Mindess et al. [66] was adopted in this study, that is, pores from 2.5 to 10 nm, from 10 to 50 nm and from 50 nm to 10 μm can be classified into small capillary (or gel) pores, medium capillary pores and large capillary pores, respectively. From Table 4, the most probable pore size and the porosity of the concrete specimens decreased with the curing age.

Table 4. Pore structures of face slab concretes added with various fly ash dosages.

Notation	Hydration Time (Day)	The Most Probable Pore Size (nm)	Porosity (%)	Pore Size Distribution		
				<10 nm (%)	10–50 nm (%)	50 nm–10 μm (%)
C0	3	176	28.5	7.9	30.6	61.2
	28	69	21.6	14.3	46.7	38.9
	180	42	19.6	18.6	49.6	31.6
CF10	3	186	30.3	7.2	27.8	64.9
	28	75	23.3	13.2	45.1	41.3
	180	38	18.2	20.3	51.2	28.3
CF20	3	197	32.6	6.7	25.6	67.5
	28	82	24.9	13	43.6	43.2
	180	33	16.5	22.5	52.5	24.8
CF30	3	212	33.7	5.6	23.1	70.6
	28	96	26.1	12.1	41.9	45.6
	180	27	14.3	24.3	53.9	21.6
CF40	3	221	35.9	4.7	21.4	73.7
	28	105	27.6	10.6	40.8	48.3
	180	25	14.1	24.2	53.6	22.1

In addition, Table 4 indicates that the fly ash addition had a noticeable influence on the pore structure parameters of face slab concrete. For instance, Table 4 displays that the fly ash addition slightly increased the three-day porosity and the average pore diameter. Specifically, CF10 concrete presented the three-day most probable pore size of 186 nm and a three-day porosity of 30.3%, which were 1.8% and 10 nm greater than those of the C0 one, respectively. Besides, a larger proportion of capillary pores (50 nm–10 μm) in concrete and a lower proportion of gel pores and medium capillary pores could also be observed for the CF10 one, indicating that the presence of fly ash coarsens the pore structures of face slab

concretes at an early age. These trends become more pronounced and evident with the increase in the fly ash dosage up to 40%, as shown in Table 4. These phenomena can be also attributed to the dilution effect and the inert nature of fly ash at an early hydration time [23–25].

As the hydration age increased from 28 to 180 days, the pore structure of face slab concrete containing fly ash turned to be more refined. For example, CF10 concrete exhibited a smaller porosity and the most probable pore size than C0 one, and CF10 also showed a smaller capillary pore proportion and a greater proportion of gel pores and medium capillary pores than the C0 one. This pore structure refinement is more notable as the fly ash dosage increases to 30%. For example, the 180-day most probable pore size and porosity were reduced from 38 nm and 18.2% for CF10 to 33 nm and 16.5% for CF20 and to 27 nm and 14.3% for CF30. These findings are owed to the pozzolanic reaction between fly ash and $\text{Ca}(\text{OH})_2$ at the long-term hydration time, which would generate secondary C-S-H to fill up the large capillary pores in concretes, resulting in a refined porous structure [14,67].

However, Table 4 shows that with the fly ash dosage increasing from 30% to 40%, this pore structure refinement was not as appreciable as that when the fly ash dosage increased from 0 to 30%. Specifically, there was no obvious difference in porosity and pore size distribution values between CF40 and CF30 concretes at 180 days. This is probably because the amount of $\text{Ca}(\text{OH})_2$ generated by cement hydration was not so sufficient for the pozzolanic reaction if the fly ash dosage approached 40%. This assumption is supported by other quantitative studies on pozzolanic reactions. For a 180-day standardly cured cement paste, the $\text{Ca}(\text{OH})_2$ fraction was about 16.7%, while it was less than 7% for a paste added with 30% fly ash [68], if the fly ash dosage increased to 40–60%, the $\text{Ca}(\text{OH})_2$ fraction in cement pastes was negligible [57]. Therefore, a fly ash dosage of 30% is optimal to refine the pore structures of face slab concretes.

3.5. Fractal Characteristics of Face Slab Concretes

Pore surface fractal dimension (D_s) values of face slab concretes added with different dosages of fly ash hydrated at 3, 28 and 180 days were calculated based on Equations (4) and (5), and the results are listed in Table 5. The fractal theories revealed that the D_s values were only meaningful between 2.0–3.0 for a porous object; a D_s approaching 3.0 means the pore structure becomes more and more complex; a D_s equal to 2 means a smooth plane, whereas an object with a D_s greater than 3 or smaller than 2 is considered to be non-fractal at all [30,69–71]. Table 5 clearly shows that all of the D_s values were in the range of 2.77 and 2.95. Hence, the pore structure of the face slab concretes containing fly ash in this study had typical fractal characteristics.

Table 5. D_s values of face slab concrete added with different fly ash dosages.

Notation	Hydration Time (Day)	D_s	R^2
C0	3	2.825	0.956
	28	2.876	0.978
	180	2.902	0.986
CF10	3	2.811	0.947
	28	2.869	0.967
	180	2.916	0.956
CF20	3	2.801	0.969
	28	2.853	0.981
	180	2.929	0.978
CF30	3	2.782	0.947
	28	2.841	0.989
	180	2.939	0.988
CF40	3	2.771	0.978
	28	2.830	0.975
	180	2.946	0.969

Additionally, the correlations between D_s and the pore structure parameters (the porosity and the most probable pore size) are illustrated in Figure 7. Many studies reported that the pores with a size smaller than 50 nm predominately affect the shrinkage development of concretes [63,72,73]. The volume fraction of such pores, which is termed as $V_{2.5-50nm}$, can be obtained by adding the fractions of medium capillary pores and gel pores. The calculated $V_{2.5-50nm}$ values are listed in Table 6. Figure 7 also displays the correlation between D_s and $V_{2.5-50nm}$.

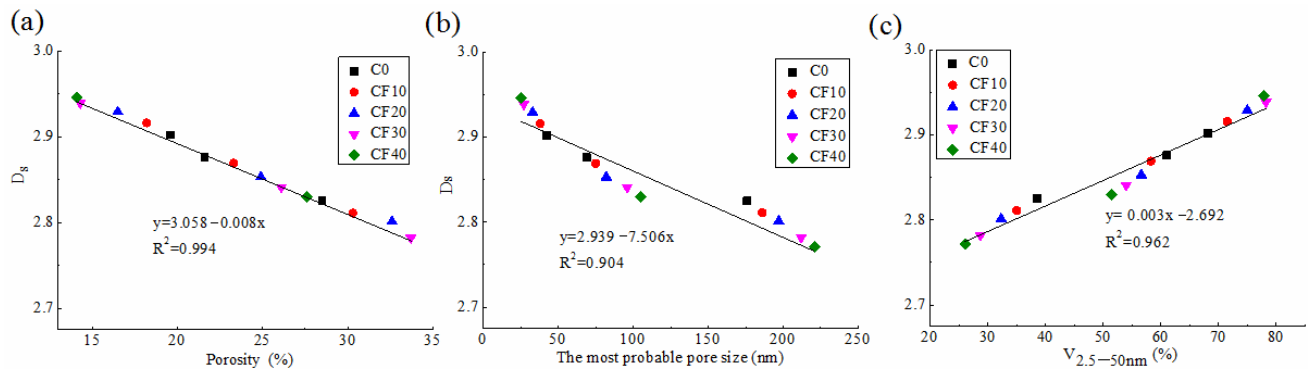


Figure 7. Correlation between D_s and (a) porosity, (b) the most probable pore size and (c) $V_{2.5-50nm}$.

Table 6. $V_{2.5-50nm}$ of face slab concrete added with different fly ash dosages.

Notation	Hydration Time (Days)	$V_{2.5-50nm}$ (%)
C0	3	38.5
	28	61.0
	180	68.2
CF10	3	35.0
	28	58.3
	180	71.5
CF20	3	32.3
	28	56.6
	180	75.0
CF30	3	28.7
	28	54.0
	180	78.2
CF40	3	26.1
	28	51.4
	180	77.8

As shown in Figure 7, the porosity, the most probable pore size and $V_{2.5-50nm}$ of face slab concretes were closely related with D_s , with high R^2 values of 0.994, 0.904 and 0.962, respectively, demonstrating that the pore structure parameters can be characterized and represented by D_s . This result corresponds well with other studies [30,31,71]. As Jin et al. [31] stated, D_s can perform more comprehensively and accurately to characterize the variations in pore structures in comparison to other pore structure parameters.

Furthermore, the correlations between D_s of concrete and the fly ash dosages are displayed in Figure 8.

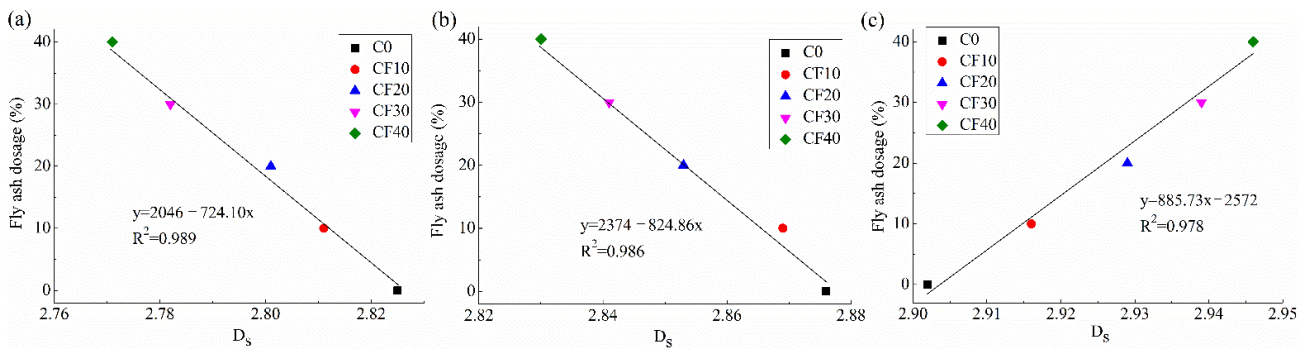


Figure 8. Correlations between D_s and fly ash dosage at (a) 3 days, (b) 28 days and (c) 180 days.

Figure 8 displays that the fly ash addition reduced the 3-day and 28-day D_s values, and the increase in fly ash dosage tended to lower the D_s values. This is because the addition of fly ash at an early age coarsens the pore structure and produces lots of large pores, as evidenced by the MIP results above.

Nevertheless, Figure 8 shows that fly ash incorporation increased the 180-day D_s values of face slab concrete, and the D_s values increased from 2.902 to 2.946 with the increase in fly ash dosage from 0 to 40%. The increase in the 180-day D_s value was caused by the reaction of fly ash at a late hydration age, which could make the pore structures of concrete more and more complex. This is a common experimental phenomenon when the mineral admixtures (e.g., silica fume [29,33] and granulated blast-furnace slag [30], etc.) are utilized in concrete, because the pozzolanic reaction of mineral admixtures could considerably intensify the complexity and irregularity of pores and thus produce high D_s values of concrete.

3.6. Pore Structural and Fractal Viewpoint of Shrinkage Behavior

3.6.1. Correlation between Shrinkage and Pore Structure

It is widely reported that the small pores with a size smaller than 50 nm significantly affect the shrinkage behavior [63,72–76]. The correlations between drying shrinkage/autogenous shrinkage of face slab concrete and $V_{2.5-50nm}$ in this work are plotted in Figures 9 and 10, respectively.

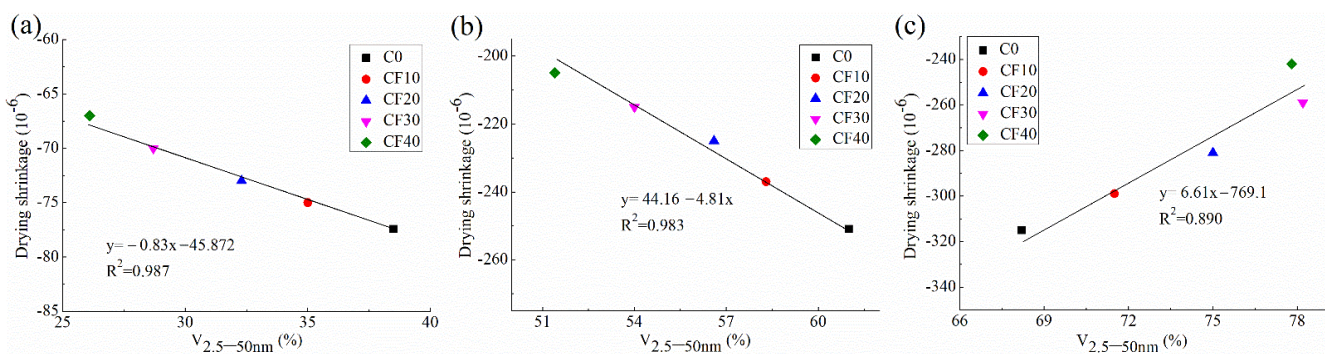


Figure 9. Correlations between drying shrinkage and $V_{2.5-50nm}$ at (a) 3 days, (b) 28 days and (c) 180 days.

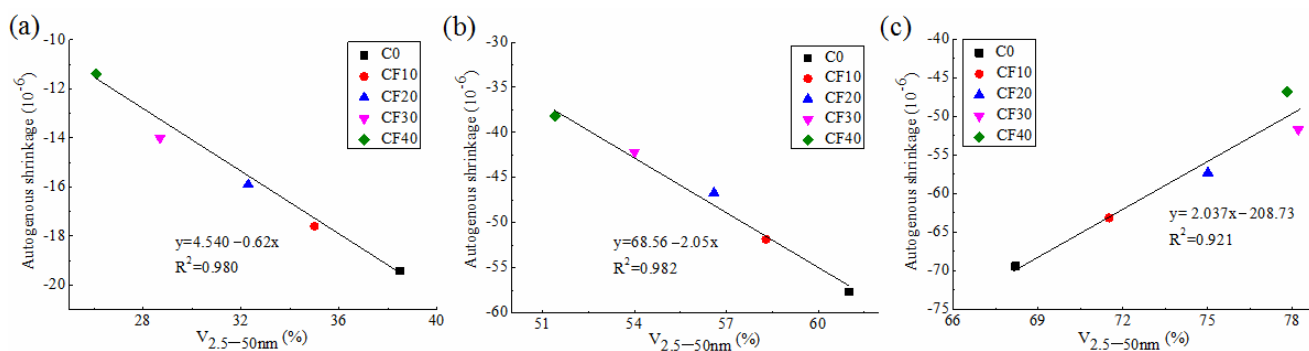


Figure 10. Correlations between autogenous shrinkage and $V_{2.5-50nm}$ at (a) 3 days, (b) 28 days and (c) 180 days.

Figures 9 and 10 illustrate that both the autogenous shrinkage and the drying shrinkage were closely correlated with the pore structure parameter $V_{2.5-50nm}$. Besides, a careful comparison of the results in Figures 9 and 10 indicate that both the autogenous shrinkage and the drying shrinkage values at 3 and 28 days increased as the $V_{2.5-50nm}$ increased. That is to say, the higher shrinkage values were accompanied by the higher fraction of small pores. This finding is consistent with the results by Li et al. [72] and Ma and Ye [63]. They demonstrated that the pores with a size ranging from 5 nm to 50 nm significantly played an important role in the shrinkage, since the capillary stresses are easy to generate within these small pores. The difference in shrinkage behavior caused by the fly ash dosage at 3 and 28 days could be explained from the viewpoint of pore structures. As revealed in Section 3.4, the fly ash addition coarsens the pores and reduces the proportions of fine pores, and the larger dosage of fly ash could further reduce the $V_{2.5-50nm}$ values. Accordingly, the lowered $V_{2.5-50nm}$ of concrete could ease the development of capillary stress in concrete, thus producing relatively low shrinkage values.

Nevertheless, a reverse trend can be observed from Figures 9 and 10, i.e., both the autogenous shrinkage and the drying shrinkage values at 180 days increased as the $V_{2.5-50nm}$ declined. This seemingly conflicting result can be explained as follows. As revealed in Section 3.3, the shrinkage of face slab concrete mainly developed before 14–28 days, because the evaporation or the cement hydration largely occur in this stage. Thereafter, the shrinkage develops rather slowly until 180 days. Although the pozzolanic reaction of fly ash at a long-term hydration time could refine the pore structures and increase the $V_{2.5-50nm}$ of concrete, the evaporation or the cement hydration at a long-term age is largely slowed down; hence, the capillary stress at this stage may not increase as rapidly as in the initial evaporation or hydration period. Besides, it has been reported that the pozzolanic reaction of fly ash at a middle and long-term age would optimize the pores and improve the resistance to shrinkage to some degrees [61,62]. Consequently, the large $V_{2.5-50nm}$ values induced by fly ash addition could not lead to large shrinkage at 180 days; hence, the relationship between shrinkage and $V_{2.5-50nm}$ at 3 and 28 days could not change at 180 days.

3.6.2. Correlation between Shrinkage and D_s

Figures 11 and 12 present the correlations of shrinkage values of face slab concretes with D_s , which are beneficial to understand the shrinkage behavior in terms of fractals.

From Figures 11 and 12, both the drying shrinkage and autogenous shrinkage of face slab concrete were closely related with D_s . They exhibited a positive correlation with D_s at 3 and 28 days, with R^2 values larger than 0.970, while they presented a negative correlation with D_s at 180 days with an R^2 of 0.990. This trend corresponds well with the relationship between concrete shrinkage and $V_{2.5-50nm}$. This can be expected because the pore structure parameter of face slab concrete in this work is closely related with D_s ; meanwhile, the pore structure parameters such as $V_{2.5-50nm}$ exhibit a close correlation with concrete shrinkage. These findings indicate that the parameter D_s plays a key role in affecting the concrete

shrinkage; that is to say, fractal theory can be employed to evaluate the shrinkage of face slab concretes.

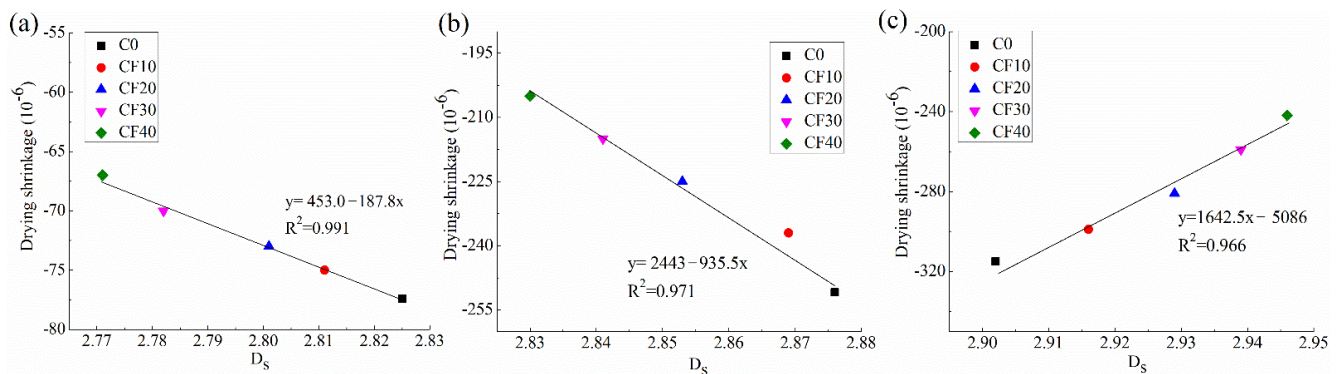


Figure 11. Correlations between drying shrinkage and D_s at (a) 3 days, (b) 28 days and (c) 180 days.

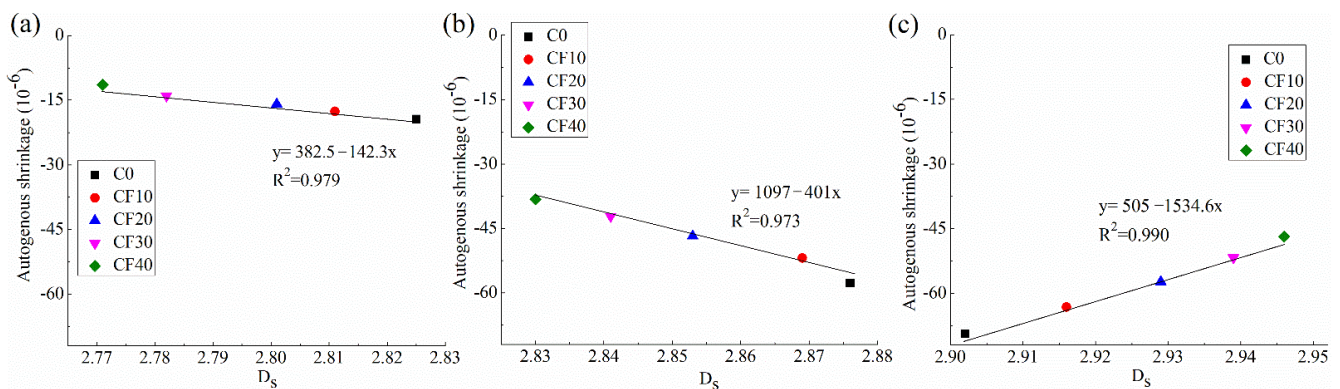


Figure 12. Correlations between autogenous shrinkage and D_s at (a) 3 days, (b) 28 days and (c) 180 days.

4. Conclusions

The following concluding remarks can be drawn in this study.

- (1) The incorporation of 10–40% fly ash could slightly reduce the drying shrinkage by about 2.2–13.5% before 14 days of hydration, and it could reduce the drying shrinkage at 180 days by about 5.1–23.2%. By contrast, the fly ash addition could largely reduce the autogenous shrinkage at early, middle and long-term ages.
- (2) Increasing fly ash dosage from 0 to 40% significantly improves the crack resistance of face slab concretes to plastic shrinkage. Nevertheless, the increase in fly ash dosage increases the drying-induced cracking risk under restrained conditions.
- (3) The pore structures of face slab concrete at 3 and 28 days become coarser with the increase in fly ash dosage up to 40%. At 180 days, the pore structures become more refined as the fly ash dosage increases to 30%; however, this refinement effect is not appreciable as the fly ash dosage increases from 30% to 40%.
- (4) The D_s of face slab concrete is strongly related with the concrete pore structures. The D_s of face slab concrete at a late age increased from 2.902 to 2.946 with increasing the fly ash dosage from 0 to 40%. The pore structure and D_s are closely correlated with the shrinkage of face slab concrete. The higher shrinkage of face slab concrete was accompanied by a higher fraction of small pores and D_s at 3 and 28 days, whereas the 180 day-shrinkage increased as the fraction of small pores and D_s declined.
- (5) A fly ash dosage around 30% is optimal for face slab concretes in terms of lowering shrinkage and refining the pore structures, without compromising much mechanical property. However, the face slab concretes with a large fly ash dosage should be well cured under restrained and evaporation conditions at an initial hydration age.

Future perspective: Further research is needed to cover a wider range of W/B ratios and more types of fly ash, as well as the comparison of the effects on shrinkage and crack resistance among fibers, MgO and fly ash.

Author Contributions: Conceptualization, writing—original draft, writing—review and editing, investigation, formal analysis, supervision, project administration and funding acquisition, L.W.; investigation, Z.Y., B.L., F.Z., S.T. and M.J. All authors have read and agreed to the published version of the manuscript.

Funding: The authors appreciate the financial support provided by the Opening Funds of the Belt and Road Special Foundation of the State Key Laboratory of Hydrology-Water Resources and Hydraulic Engineering (funding number: 2020492311).

Data Availability Statement: The data that support the findings of this study are available from the corresponding author upon reasonable request.

Acknowledgments: The authors would like to thank all the anonymous referees for their constructive comments and suggestions.

Conflicts of Interest: The authors declare no conflict of interest.

References

1. Qu, Y.Q.; Zou, D.G.; Kong, X.J.; Liu, J.M.; Zhang, Y.; Yu, X. Seismic damage performance of the steel fiber reinforced face slab in the concrete-faced rockfill dam. *Soil Dyn. Earthq. Eng.* **2019**, *119*, 320–330. [[CrossRef](#)]
2. Kong, X.J.; Zhang, Y.; Zou, D.G.; Yong, Q.; Xiang, Y.U. Seismic cracking analyses of two types of face slab for concrete-faced rockfill dams. *Sci. China Technol. Sc.* **2017**, *60*, 510–522. [[CrossRef](#)]
3. Ma, H.Q.; Chi, F.D. Technical progress on researches for the safety of high concrete-faced rockfill dams. *Engineering* **2016**, *2*, 332–339. [[CrossRef](#)]
4. Cen, W.J.; Wen, L.S.; Zhang, Z.Q.; Xiong, K. Numerical simulation of seismic damage and cracking of concrete slabs of high concrete face rockfill dams. *Water Sci. Technol.* **2016**, *9*, 205–211. [[CrossRef](#)]
5. Wang, Z.J.; Liu, S.H.; Vallejo, L.; Wang, L.J. Numerical analysis of the causes of face slab cracks in Gongboxia rockfill dam. *Eng. Geol.* **2014**, *181*, 224–232. [[CrossRef](#)]
6. Oskouei, A.V.; Nazari, R.; Khaneghahi, M.H. Laboratory and in situ investigation of the compressive strength of CFRD concrete. *Constr. Build. Mater.* **2020**, *242*, 118166. [[CrossRef](#)]
7. Jia, J.S. A technical review of hydro-project development in China. *Engineering* **2016**, *2*, 302–312. [[CrossRef](#)]
8. Yang, Z.Y.; Chao, L.; Wu, M.X. Leading-edge technologies in hydropower development in China. *Glob. Energy Interconnect.* **2019**, *2*, 244–253. [[CrossRef](#)]
9. Woo, S.K.; Song, Y.C.; Won, J.P. Enhanced durability performance of face slab concrete in Concrete-Faced Rock-filled Dam using fly ash and PVA fibre. *KSEC J. Civ. Eng.* **2011**, *15*, 875–882. [[CrossRef](#)]
10. Zhou, W.; Hua, J.; Chang, X.; Zhou, C. Settlement analysis of the Shuibuya concrete-face rockfill dam. *Comput. Geotech.* **2011**, *38*, 269–280. [[CrossRef](#)]
11. Baak, S.H.; Cho, G.C.; Song, K.I. Stability analysis on the concrete slab of the highest concrete-faced rock-fill dam in South Korea. *Geomech. Eng.* **2017**, *13*, 881–892.
12. Altoubat, S.; Talha Junaid, M.; Leblouba, M.; Badran, D. Effectiveness of fly ash on the restrained shrinkage cracking resistance of self-compacting concrete. *Cem. Concr. Compos.* **2017**, *79*, 9–20. [[CrossRef](#)]
13. Wongkeo, W.; Thongsanitgarn, P.; Chaipanich, A. Compressive strength and drying shrinkage of fly ash-bottom ash-silica fume multi-blended cement mortars. *Mater. Des.* **2012**, *36*, 655–662. [[CrossRef](#)]
14. Termkhajornkit, P.; Nawa, T.; Nakai, M.; Saito, T. Effect of fly ash on autogenous shrinkage. *Cem. Concr. Res.* **2005**, *35*, 473–482. [[CrossRef](#)]
15. Kristiawan, S.A.; Aditya, M.T.M. Effect of high volume fly ash on shrinkage of self-compacting concrete. *Procedia Eng.* **2015**, *125*, 705–712. [[CrossRef](#)]
16. Hu, X.; Shi, C.J.; Shi, Z.G.; Tong, B.H.; Wang, D.H. Early age shrinkage and heat of hydration of cement-fly ash-slag ternary blends. *Constr. Build. Mater.* **2017**, *153*, 857–865. [[CrossRef](#)]
17. Bouchenafa, O.; Hamzaoui, R.; Bennabi, A.; Colin, J. PCA effect on structure of fly ashes and slag obtained by mechanosynthesis. Applications: Mechanical performance of substituted paste CEMI + 50% slag/or fly ashes. *Constr. Build. Mater.* **2019**, *203*, 120–133. [[CrossRef](#)]
18. Wang, L.; He, Z.; Cai, X.H. Characterization of pozzolanic reaction and its effect on the C-S-H gel in fly ash-cement paste. *J. Wuhan Univ. Technol.* **2011**, *26*, 320–325. [[CrossRef](#)]
19. Yang, B.B.; Liu, J.W.; Zhao, X.M.; Zheng, S. Evaporation and cracked soda soil improved by fly ash from recycled materials. *Land Degrad. Dev.* **2021**, *32*, 2823–2832. [[CrossRef](#)]

20. Zhang, P.; Wang, K.X.; Wang, J.; Guo, J.J.; Ling, Y.F. Macroscopic and microscopic analyses on mechanical performance of metakaolin/fly ash based geopolymer mortar. *J. Clean. Prod.* **2021**, *294*, 126193. [[CrossRef](#)]
21. Nath, P.; Sarker, P. Effect of fly ash on the durability properties of high strength concrete. *Procedia Eng.* **2011**, *14*, 1149–1156. [[CrossRef](#)]
22. Hu, X.; Shi, Z.G.; Shi, C.J.; Wu, Z.M.; Tong, B.H.; Ou, Z.H.; de Schutter, G. Drying shrinkage and cracking resistance of concrete made with ternary cementitious components. *Constr. Build. Mater.* **2017**, *149*, 406–415. [[CrossRef](#)]
23. Atis, C.D. Heat evolution of high-volume fly ash concrete. *Cem. Concr. Res.* **2002**, *32*, 751–756. [[CrossRef](#)]
24. Wang, L.; Yang, H.Q.; Zhou, S.H.; Chen, E.; Tang, S.W. Mechanical properties, long-term hydration heat, shrinkage behavior and crack resistance of dam concrete designed with low heat Portland (LHP) cement and fly ash. *Constr. Build. Mater.* **2018**, *187*, 1073–1091. [[CrossRef](#)]
25. Yin, B.; Kang, T.; Kang, J.; Chen, Y.; Wu, L.; Du, M. Investigation of the hydration kinetics and microstructure formation mechanism of fresh fly ash cemented filling materials based on hydration heat and volume resistivity characteristics. *Appl. Clay Sci.* **2018**, *166*, 146–158. [[CrossRef](#)]
26. *DL/T 5016-2011*; Design Code for Concrete Faced Rockfill Dams, China. China Electric Power Press: Beijing, China, 2011.
27. Bin, L.; Wang, L.; Zhou, S.; Liu, S. Research on mechanical properties and crack resistance of concrete slab under compound addition of fly ash and PVA fiber. *Yangtze River* **2018**, *49*, 84–87. (In Chinese) [[CrossRef](#)]
28. Yoon, Y.S.; Won, J.P.; Woo, S.K. Enhanced durability performance of fly ash concrete for concrete-faced rockfill dam application. *Cem. Concr. Res.* **2002**, *32*, 23–30. [[CrossRef](#)]
29. Zarnaghi, V.N.; Ali, F.A.; Nourani, V.; Ma, H.Y. On the pore structures of lightweight self-compacting concrete containing silica fume. *Constr. Build. Mater.* **2018**, *193*, 557–564. [[CrossRef](#)]
30. Zeng, Q.; Luo, M.Y.; Pang, X.Y.; Li, L.; Li, K.F. Surface fractal dimension: An indicator to characterize the microstructure of cement-based porous materials. *Appl. Surf. Sci.* **2013**, *282*, 302–307. [[CrossRef](#)]
31. Jin, S.S.; Zhang, J.X.; Han, S. Fractal analysis of relation between strength and pore structure of hardened mortar. *Constr. Build. Mater.* **2017**, *135*, 1–7. [[CrossRef](#)]
32. Yu, P.; Duan, Y.H.; Chen, E.; Tang, S.W.; Wang, X.R. Microstructure-based fractal models for heat and mass transport properties of cement paste. *Int. J. Heat Mass Transf.* **2018**, *126*, 432–447. [[CrossRef](#)]
33. Lü, Q.; Qiu, Q.L.; Zheng, J.; Wang, J.Y.; Zeng, Q. Fractal dimension of concrete incorporating silica fume and its correlations to pore structure, strength and permeability. *Constr. Build. Mater.* **2019**, *228*, 116986. [[CrossRef](#)]
34. Yang, B.B.; Li, D.D.; Yuan, S.C.; Jin, L.C. Role of biochar from corn straw in influencing crack propagation and evaporation in sodic soils. *Catena* **2021**, *204*, 105457. [[CrossRef](#)]
35. Zhang, P.; Gao, Z.; Wang, J.; Wang, K. Numerical modeling of rebar-matrix bond behaviors of nano-SiO₂ and PVA fiber reinforced geopolymer composites. *Ceram. Int.* **2021**, *47*, 11727–11737. [[CrossRef](#)]
36. Zhang, P.; Wang, K.X.; Wang, J.; Guo, J.J.; Hu, S.W.; Ling, Y.F. Mechanical properties and prediction of fracture parameters of geopolymer/alkali-activated mortar modified with PVA fiber and nano-SiO₂. *Ceram. Int.* **2020**, *46*, 20027–20037. [[CrossRef](#)]
37. Jin, S.S.; Zhang, J.X.; Huang, B.S. Fractal analysis of effect of air void on freeze–thaw resistance of concrete. *Constr. Build. Mater.* **2013**, *47*, 126–130. [[CrossRef](#)]
38. *DL/T 5330-2015*; Code for Mix Design of Hydraulic Concrete, China. China Electric Power Press: Beijing, China, 2015.
39. *DL/T 5150-2017*; Test Code for Hydraulic Concrete, China. China Electric Power Press: Beijing, China, 2017.
40. Banthia, N.; Gupta, R. Influence of polypropylene fiber geometry on plastic shrinkage cracking in concrete. *Cem. Concr. Res.* **2006**, *36*, 1263–1267. [[CrossRef](#)]
41. Khan, I.; Castel, A.; Gilbert, R.I. Tensile creep and early-age concrete cracking due to restrained shrinkage. *Constr. Build. Mater.* **2017**, *149*, 705–715. [[CrossRef](#)]
42. Al-Amoudi, O.S.B.; Maslehuddin, M.; Shameem, M.; Ibrahim, M. Shrinkage of plain and silica fume cement concrete under hot weather. *Cem. Concr. Compos.* **2007**, *29*, 690–699. [[CrossRef](#)]
43. Rao, G.A. Long-term drying shrinkage of mortar-influence of silica fume and size of fine aggregate. *Cem. Concr. Res.* **2001**, *31*, 171–175. [[CrossRef](#)]
44. *CCES 01-2004*; Design and Construction Guide for the Durability of Concrete Structures, China. China Civil Engineering Society Press: Beijing, China, 2004.
45. Yousefieh, N.; Joshaghani, A.; Hajibandeh, E.; Shekarchi, M. Influence of fibers on drying shrinkage in restrained concrete. *Constr. Build. Mater.* **2017**, *148*, 833–845. [[CrossRef](#)]
46. *ASTM C1581/C1581M-16*; Standard Test Method for Determining Age at Cracking and Induced Tensile Stress Characteristics of Mortar and Concrete under Restraint Shrinkage. ASTM International: West Conshohocken, PA, USA, 2016.
47. Shen, D.J.; Kang, J.C.; Yi, X.J.; Zhou, L.K.; Shi, X. Effect of double hooked-end steel fiber on early-age cracking potential of high strength concrete in restrained ring specimens. *Constr. Build. Mater.* **2019**, *223*, 1095–1105. [[CrossRef](#)]
48. Wang, L.; Yang, H.Q.; Dong, Y.; Chen, E.; Tang, S.W. Environmental evaluation, hydration, pore structure, volume deformation and abrasion resistance of low heat Portland (LHP) cement-based materials. *J. Clean. Prod.* **2018**, *203*, 540–558. [[CrossRef](#)]
49. Yang, B.; Liu, Y. Application of fractals to evaluate fractures of rock due to mining. *Fractal Fract.* **2022**, *6*, 96. [[CrossRef](#)]
50. Zhang, B.Q.; Li, S.F. Determination of the surface fractal dimension for porous media by mercury porosimetry. *Ind. Eng. Chem. Res.* **1995**, *34*, 1383–1386. [[CrossRef](#)]

51. Zhang, B.Q.; Liu, W.; Liu, X. Scale-dependent nature of the surface fractal dimension for bi- and multi-disperse porous solids by mercury porosimetry. *Appl. Surf. Sci.* **2006**, *253*, 1349–1355. [[CrossRef](#)]
52. Bouzoubaâ, N.; Zhang, M.H.; Malhotra, V.M. Mechanical properties and durability of concrete made with high-volume fly ash blended cements using a coarse fly ash. *Cem. Concr. Res.* **2001**, *31*, 1393–1402. [[CrossRef](#)]
53. De Matos, P.R.; Foiato, M.; Prudencio, L.R., Jr. Studies of the physical properties of hardened Portland cement paste—Part 8. The freezing of water in hardened Portland cement paste. *Constr. Build. Mater.* **2019**, *203*, 282–293.
54. Termkhajornkit, P.; Nawa, T.; Kurumisawa, K. Effect of water curing conditions on the hydration degree and compressive strengths of fly ash–cement paste. *Cem. Concr. Compos.* **2006**, *28*, 781–789. [[CrossRef](#)]
55. Jiang, D.B.; Li, X.G.; Lv, Y.; Zhou, M.K.; Li, C.J. Utilization of limestone powder and fly ash in blended cement: Rheology, strength and hydration characteristics. *Constr. Build. Mater.* **2020**, *232*, 117228. [[CrossRef](#)]
56. Poon, C.S.; Lam, L.; Wong, Y.L. A study on high strength concrete prepared with large volumes of low calcium fly ash. *Cem. Concr. Res.* **2000**, *30*, 447–455. [[CrossRef](#)]
57. Sakai, E.; Miyahara, S.; Ohsawa, S.; Lee, S.H.; Daimon, M. Hydration of fly ash cement. *Cem. Concr. Res.* **2005**, *35*, 1135–1140. [[CrossRef](#)]
58. Oner, A.; Akyuz, S.; Yildiz, R. An experimental study on strength development of concrete containing fly ash and optimum usage of fly ash in concrete. *Cem. Concr. Res.* **2005**, *35*, 1165–1171. [[CrossRef](#)]
59. Yang, J.; Huang, J.X.; He, X.Y.; Su, Y.; Oh, S.K. Shrinkage properties and microstructure of high volume ultrafine phosphorous slag blended cement mortars with superabsorbent polymer. *J. Build. Eng.* **2020**, *52*, 101121. [[CrossRef](#)]
60. Deboodt, T.; Fu, T.; Ideker, J.H. Evaluation of FLWA and SRAs on autogenous deformation and long-term drying shrinkage of high performance concrete. *Constr. Build. Mater.* **2016**, *119*, 53–60. [[CrossRef](#)]
61. Haneef, T.K.; Kumari, K.; Mukhopadhyay, C.K.; Venkatachalapathy; Rao, B.P.; Jayakumar, T. Influence of fly ash and curing on cracking behavior of concrete by acoustic emission technique. *Constr. Build. Mater.* **2013**, *44*, 342–350. [[CrossRef](#)]
62. Gökçe, H.S.; Hatungimana, D.; Ramyar, K. Effect of fly ash and silica fume on hardened properties of foam concrete. *Constr. Build. Mater.* **2019**, *194*, 1–11. [[CrossRef](#)]
63. Ma, Y.; Ye, G. The shrinkage of alkali activated fly ash. *Cem. Concr. Res.* **2015**, *68*, 75–82. [[CrossRef](#)]
64. Yang, R.; Yu, R.; Shui, Z.H.; Gao, X. Low carbon design of an ultra-high performance concrete (UHPC) incorporating phosphorous slag. *J. Clean. Prod.* **2019**, *240*, 118157. [[CrossRef](#)]
65. Moghaddam, F.; Sirivivatnanon, V.; Vessalas, K. The effect of fly ash fineness on heat of hydration, microstructure, flow and compressive strength of blended cement pastes. *Case Stud. Constr. Mater.* **2019**, *10*, e00218. [[CrossRef](#)]
66. Mindess, S.; Young, J.F.; Darwin, D. *Concrete*; Prentice-Hall: Murray Hill, NJ, USA, 2003.
67. Zhang, Y.M.; Sun, W.; Yan, H.D. Hydration of high-volume fly ash cement pastes. *Cem. Concr. Compos.* **2000**, *22*, 445–452. [[CrossRef](#)]
68. Wang, L.; Dong, Y.; Zhou, S.H.; Chen, E.; Tang, S.W. Energy saving benefit, mechanical performance, volume stabilities, hydration properties and products of low heat cement-based materials. *Energy Build.* **2018**, *170*, 157–169. [[CrossRef](#)]
69. Liu, P.; Cui, S.; Li, Z.; Xu, X.; Guo, C. Influence of surrounding rock temperature on mechanical property and pore structure of concrete for shotcrete use in a hot-dry environment of high-temperature geothermal tunnel. *Constr. Build. Mater.* **2019**, *207*, 329–337. [[CrossRef](#)]
70. Xie, H.; Ni, G.; Li, S. The influence of surfactant on pore fractal characteristics of composite acidized coal. *Fuel* **2019**, *253*, 741–753. [[CrossRef](#)]
71. Zeng, Q.; Li, K.F.; Teddy, F.C.; Patrick, D.L. Surface fractal analysis of pore structure of high-volume fly-ash cement pastes. *Appl. Surf. Sci.* **2010**, *257*, 762–768. [[CrossRef](#)]
72. Li, Y.; Bao, J.; Guo, Y. The relationship between autogenous shrinkage and pore structure of cement paste with mineral admixtures. *Constr. Build. Mater.* **2010**, *24*, 1855–1860. [[CrossRef](#)]
73. Zhang, W.; Ha, Y.; Na, S.H. Drying shrinkage and microstructure characteristics of mortar incorporating ground granulated blast furnace slag and shrinkage reducing admixture. *Constr. Build. Mater.* **2015**, *93*, 267–277. [[CrossRef](#)]
74. Yuan, B.; Li, Z.; Zhao, Z.; Ni, H.; Su, Z. Experimental study of displacement field of layered soils surrounding laterally loaded pile based on Transparent Soil. *J. Soils Sediments* **2021**, *21*, 3072–3083. [[CrossRef](#)]
75. Yuan, B.; Li, Z.; Chen, Y.; Ni, H.; Zhao, Z.; Chen, W. Mechanical and microstructural properties of recycling granite residual soil reinforced with glass fiber and liquid-modified polyvinyl alcohol polymer. *Chemosphere* **2021**, *268*, 131652. [[CrossRef](#)]
76. Yuan, B.; Sun, M.; Wang, Y.; Zhai, L.; Luo, Q.; Zhang, X. Full 3D displacement measuring system for 3D displacement field of soil around a laterally loaded pile in transparent soil. *Int. J. Geomech.* **2019**, *19*, 04019028. [[CrossRef](#)]